Confinement of surface waves at the air-water interface to control aerosol size and dispersity

Elijah Nazarzadeh, Rab Wilson, Xi King, Julien Reboud, Manlio Tassieri, and Jonathan M. Cooper

Citation: Physics of Fluids **29**, 112105 (2017);
View online: https://doi.org/10.1063/1.4993793
View Table of Contents: http://aip.scitation.org/toc/phf/29/11
Published by the American Institute of Physics

PHYSICS OF FLUIDS **29**, 112105 (2017)

Confinement of surface waves at the air-water interface to control aerosol size and dispersity

Elijah Nazarzadeh,[a] Rab Wilson, Xi King, Julien Reboud, Manlio Tassieri, and Jonathan M. Cooper[a]
Division of Biomedical Engineering, University of Glasgow, Rankine Building, Glasgow G12 8LT, United Kingdom

(Received 30 June 2017; accepted 12 October 2017; published online 15 November 2017)

The precise control over the size and dispersity of droplets, produced within aerosols, is of great interest across many manufacturing, food, cosmetic, and medical industries. Amongst these applications, the delivery of new classes of high value drugs to the lungs has recently attracted significant attention from pharmaceutical companies. This is commonly achieved through the mechanical excitation of surface waves at the air liquid interface of a parent liquid volume. Previous studies have established a correlation between the wavelength on the surface of liquid and the final aerosol size. In this work, we show that the droplet size distribution of aerosols can be controlled by constraining the liquid inside micron-sized cavities and coupling surface acoustic waves into different volumes of liquid inside micro-grids. In particular, we show that by reducing the characteristic physical confinement size (i.e., either the initial liquid volume or the cavities' diameters), higher harmonics of capillary waves are revealed with a consequent reduction of both aerosol mean size and dispersity. In doing so, we provide a new method for the generation and fine control of aerosols' sizes distribution. https://doi.org/10.1063/1.4993793

I. INTRODUCTION

Surface acoustic waves (SAWs) can be generated by means of interdigitated transducers (IDTs) on the surface of a piezoelectric material to create a Rayleigh wave of nanometers in amplitude.[1] These waves can couple into thin plates, placed on the piezoelectric material, where they propagate as Lamb waves.[2] When a liquid is placed in the propagation path of such waves, on a thin plate, the ultrasonic wave refracts into the fluid with a transfer of mechanical energy and radiative pressure that leads to fluid streaming, Fig. 1.

This phenomenon has led to many new processes including centrifugation,[1] pumping,[3] mixing,[4] and most relevant to this work, nebulisation[3,5,6] (leading to the dispersion of the liquid as an aerosol of micro-droplets at an air-liquid interface).[7] Nebulisation has many industrial and medical applications including surface coating,[8] printing of protein microarrays,[9] combustion,[10] spray drying,[11] mass spectrometry,[12,13] nanoparticles synthesis,[14] and drug dispensation through nebulisers[15–17] for the treatment of pulmonary diseases.[18–21] In all cases, obtaining precise control of the droplet size is crucial to achieve a consistent and reproducible delivery of the aerosols. For instance, it has been shown that for an efficient and effective drug delivery to the lungs, a narrow distribution of aerosol droplet diameters between 1 and 5 μm is required.[20,21]

The first studies on drop formation from the surface of a liquid were carried out by Beer,[22] Plateau,[23] and Lord Rayleigh.[24,25] They observed that the propagation of waves on a liquid jet forms bulges and necks with positive and negative pressures, forming instability waves on the jet. The liquid jet breaks up into droplets when the instability wavelength exceeds a critical value (λ_{Cr}).[26] These studies underpin our current understanding of drop formation due to instabilities at a liquid interface, which have since found many applications.[27–31]

Surface wave parameters at the air-liquid interface (e.g., frequency and wavelength) can be understood according to the wave dispersion theory. In particular, by considering a two-dimensional wave traveling on the surface of a liquid in the x direction, as $y = \eta(x, t) = A\cos(kx - \omega t)$, where k ($=2\pi/\lambda$) is the wavenumber and ω is the angular surface wave frequency, the wave velocity dispersion is obtained,[32,33]

$$\omega^2 = \left(kg + \frac{\gamma k^3}{\rho}\right)\tanh kh, \tag{1}$$

where γ, ρ, g, and h are the surface tension, the liquid density, the gravitational acceleration, and liquid depth, respectively. The first term in Eq. (1) within the bracket is the wave dispersion due to the gravitational force, whereas the second term is due to the capillary force. The crossover frequency from gravity wave to capillary wave occurs at $k^* = \sqrt{g\rho/\gamma}$ and is equal to $\omega^* = \sqrt[4]{4g^3\,\rho/\gamma}$.[34] The capillary length ($1/k^*$) can also be used to define the boundary between regimes of influence from gravitational and capillary forces. The capillary length for water is 2.7 mm, and the capillary force is dominant in liquid bodies smaller than 2.7 mm (which is true for the cases studied in this work).

[a]Authors to whom correspondence should be addressed: Jon.Cooper@glasgow.ac.uk and Elijah.Nazarzadeh@glasgow.ac.uk

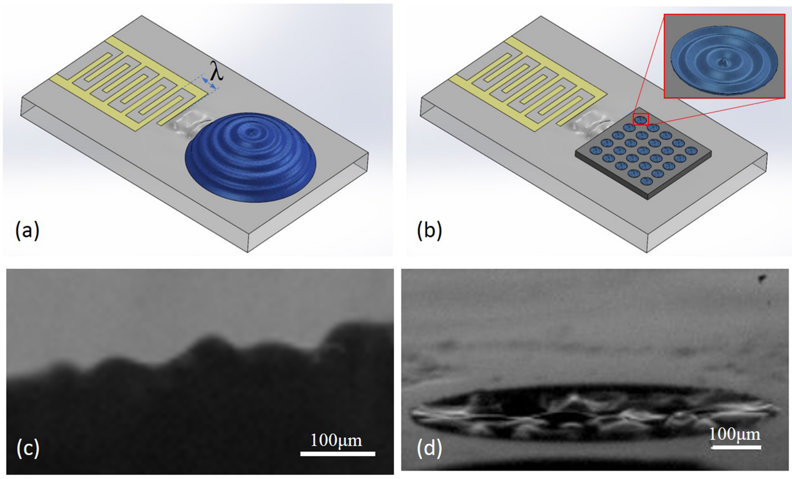

FIG. 1. (a) A schematic representation of the SAW induced vibrations on the surface of an excited lithium niobate and the subsequent excited surface waves on the surface of a free liquid droplet. (b) A schematic representation of a low pass filter coupled to the surface of a SAWs device. (c) Close-up of surface waves formed on the surface of a free liquid droplet of 2 μl volume with SAWs excited at a frequency of 9.7 MHz and a power of 1 W. (d) Surface waves formed on the surface of a confined liquid inside a microcavity (i.e., the filter) of 1500 μm in diameter; SAWs were excited at a frequency of 9.7 MHz and a power of 2 W.

Previous studies using SAWs as nebulisers have already shown a direct correlation between the median diameter of the aerosol droplets (d_m) and both the dimension of the surface waves at the air-water interface and the acoustic excitation frequency (f).[35] Early studies, using bulk acoustic waves with low frequency ultrasonic nebulisation (<1 MHz), also indicate a correlation between the average droplet size and the frequency of the surface waves (f_c) formed on the liquid surface.[35,36] Based on the assumption first proposed by Kelvin[37,38] that $f_c = f/2$ and by replacing $k = 2\pi/\lambda$ and $\omega = 2\pi f$ into the wave dispersion equation (i.e., $\omega^2 = \frac{\gamma k^3}{\rho}$), the capillary wavelength (λ_c) becomes[35,38]

$$d_m \propto \lambda_c = \left(\frac{8\pi\gamma}{\rho f^2}\right)^{1/3}, \tag{2}$$

where f is the ultrasound excitation frequency. Lang[35] validated this correlation, which was also derived by other authors.[31,39–41] However, recent studies suggest that Kelvin's assumption on the capillary frequency (i.e., $f_c = f/2$) is not valid for high frequency excitations.[42] This is mainly due to the fact that the low frequencies used in early studies are comparable to the natural oscillation frequency of the fluid body (i.e., ~kHz),[43,44] thus leading to confusion between the two.

In general, depending upon the geometry of the parent drop [e.g., diameter of a spherical cap droplet, Fig. 1(a)], nebulisation occurring through SAWs gives rise to an aerosol with a multimodal size distribution.[7,41,42] This has been explained by the acoustic deformation of the liquid volume, creating a thin layer of liquid adjacent to the bulk of the fluid, which results in the generation of small droplets (<10 μm), while larger droplets (>10 μm) detach from the bulk of the liquid. These studies conclude that the final droplet size of the nebulised liquid depends on the characteristic length scale of the liquid within the SAW propagation path, which could be either its width or its height.[45]

The dependence of droplet size on liquid length can also be corroborated from the capillary dispersion equation by considering that the largest wavelength can only be equal to the diameter of the initial liquid volume (i.e., $\lambda \cong 2R$). Therefore, the capillary dispersion relationship [i.e., second term in Eq. (1)] also provides a linkage between the surface or capillary wave frequency and liquid length scale (i.e., diameter) as $\omega \propto (\gamma/\rho R^3)^{0.5}$, where the characteristic length scale in this communication refers to the width (i.e., the diameter) of the body of the liquid.

In this work, we present a method to control the final aerosol droplet size and its dispersity by restricting the generation of low frequency surface waves [Figs. 1(b) and 1(d)] within micro-fabricated cavities. These physical structures act as low pass (cutoff) filters and confine the surface waves through imposing a characteristic (and defined) length scale to the nebulisation system. In doing so, we are able to provide experimental evidence that the wavelength of the surface waves at liquid-air interface is strongly correlated to the length scale of the liquid placed on the propagation path of SAWs, such that a precise control over the aerosol size distribution is achieved. In Sec. III A, we discuss the dependence of the wavelength of the surface waves, created by acoustic actuation of the fluid, on liquid length scale. After studying this correlation, we show how physical confinement can act as a filter to control the surface waves (Sec. III B). This is achieved by using low amounts in actuation powers in order to visualise the waves generated. The resulting droplet size in an aerosol created from non-confined and confined liquid at powers sufficient to nebulise is presented in Sec. III C.

II. METHODS AND MATERIALS

A. SAW device fabrication and nebulisation

SAWs were generated on the surface of the piezoelectric lithium niobate ($LiNbO_3$) using an interdigitated transducer (IDT), as schematically shown in Fig. 1. The IDT comprised of 30 straight finger pairs of gold (70 nm) on titanium (10 nm), with an aperture of 1 cm, patterned using a lift-off process on a 1 mm thick 128° Y-cut X-propagating $LiNbO_3$ wafer by standard photolithography. After processing, the IDT was subjected to plasma ashing for 120 s at 100 W (Plasma Fab 505 Barrel Asher, UK) and stored at room temperature. The water contact angle on the $LiNbO_3$ was 45° ± 5°.

Cylindrical cavities were etched in Si, with diameters of 100, 200, 400, 600, 800, and 1500 μm. The silicon wafer was patterned using a standard photolithography and dry etched to a depth (y) of 250 μm. The silicon chips were then treated in Piranha solution for 60 s, followed by plasma ashing (120 s at 100 W) to produce a hydrophilic surface with a contact angle of $40° \pm 5°$. The resulting silicon chip (22×22 mm) was then coupled to the $LiNbO_3$ surface, as a thin plate [Fig. 1(b)], using a small volume (ca. 10 μl) of ultrasound transmission gel (Aquasonic 100, Parker Laboratories, INC., USA). The cavities were fully filled with water before conducting each experiment.

The SAW actuated nebulisation was performed using different volumes of deionised water in droplets with volumes between 0.5 and 2.0 μl. The length scale of sessile drops of 2.0, 1.5, 1.0, and 0.5 μl is roughly 1.6, 1.4, 1.2, and 1.0 mm, respectively. The aspect ratio (height to length) of these sessile droplets is 0.2 ± 0.05. A high-speed camera (Phantom V2511, Vision Research, USA) captured images in order to monitor formation of surface waves, measure the wavelength [from peak-to-peak, Figs. 1(a) and 1(c)], and monitor the nebulisation process. Several hundred measurements were carried out for the waves on the surface of both free and confined liquids [Figs. 1(a)–1(d)]. Images were acquired at a frame rate of 100 000 s^{-1} with a resolution of 384×288 pixels, unless otherwise stated. Pixel to micrometer calibrations were performed using a graticule (5.38 ± 0.02 μm/pixel). The occurrence frequency of surface waves with different wavelengths was calculated using bin sizes of 50 μm (Fig. 2). The mean value of these waves is presented as white markers; while the rest of the distribution is presented as a scatter plot.

A laser diffraction instrument (Spraytec, Malvern, UK) was used to measure the aerosol droplet size distribution. This method is capable of measuring droplet sizes of 0.1–2000 μm in diameter. In all cases, the mean value of 3 replicates is reported.

III. RESULTS AND DISCUSSIONS

A. Free sessile drop

The relationship between a characteristic length in the liquid and how it scales with the SAW induced surface waves at the air-water interface was explored either by placing a sessile (free) drop on the lithium niobate wafer in the propagation path of SAW [Fig. 1(a)] or by constraining the liquid within a micro-structured filter [Fig. 1(b)]. In both cases, as the SAW reaches the liquid, it refracts into the fluid as a longitudinal pressure wave. The mechanical energy of the vibration, carried by the acoustic wave, partially transfers into the liquid and produces streaming inside the droplet, and generates waves on the free surface of the liquid [Figs. 1(a) and 1(c)].[46,47] This flow inside the droplet can be characterised by the Reynolds number: $Re_s = \rho uR/\mu$, where u is the streaming velocity inside the droplet (ca. 10^{-1}-10 m s^{-1}, measured using microscopy analysis[48]), R is the droplet radius (ca. 10^{-3} m), and μ is the fluid's dynamic viscosity (water, ca. 10^{-3} Pa s). It was estimated that $Re_s > 10^2$, the given threshold for turbulent streaming.[47] Turbulent surface waves have been observed on the free surface of the water droplet, producing sub-harmonic cascades of surface waves.[47,49]

The term "surface waves" on the liquid surface is used to describe the "capillary surface waves" [Fig. 1(c)]. The mean values of the measured wavelength distributions are presented in Fig. 2(a) (white squares). They show proportionality with the characteristic length scale of fluid (i.e., the diameter of the sessile drop). From Fig. 2(b), it is possible to see that the number of waves longer than 500 μm decreases sharply when the characteristic length scale is decreased from 1.6 mm to 1.4 mm. Moreover, a further decrease in the characteristic length scale results in the formation of a smaller number of long waves (>350 μm) and a higher number of short waves (<150 μm).

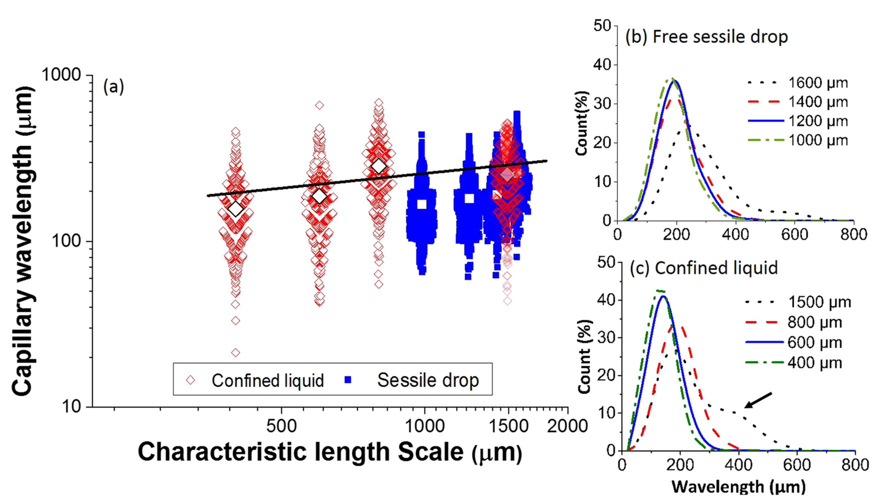

FIG. 2. (a) The mean wavelength against the characteristic length scale (droplet diameter for free sessile drops on the surface of lithium niobate—blue squares; confinement diameter for a liquid confined by the filters—red diamonds). The volume and length scale for different volumes of sessile drops is 2.0, 1.5, 1.0, and 0.5 μl to 1.6, 1.4, 1.2, and 1.0 mm, respectively. The input power is 2 W. The black line is a guide for the power law $L^{1/4}$. The width of the scatter plots is to ease reading and does not represent measurement—each population is only linked to one characteristic length scale. (b) and (c) show the measured wavelength distribution for sessile droplets and liquid confined in cavities. (b) Variation in the wavelength spectrum (bin size 50 μm) with liquid length scale; dotted black line: 1.6 mm (2.0 μl); dashed red line: 1.4 mm (1.5 μl); solid blue line: 1.2 mm (1.0 μl); and dash-dotted green line: 1.0 mm (0.5 μl). (c) Wavelength spectrum for confined liquids in cavities with different diameters; black dotted line: 1500 μm; red dashed line: 800 μm; solid blue line: 600 μm; and green dotted-dashed line: 400 μm.

A second significant parameter that determines the size of the surface waves is the acoustic power (P) of the vibrational actuation. As the power was increased, we observed the formation of shorter surface waves, blue squares in Fig. 3(a). The decrease in wavelength size was modest at lower power inputs (i.e., from 0.3 to 0.6 W); however, a further increase in power significantly diminished the formation of waves larger than 600 and 450 μm, for 1.0 and 2.0 W energy input, respectively. This also resulted in an increase in the number of short waves [~150 μm, Fig. 3(b)].

This phenomenon of creating shorter surface waves at higher powers can be analysed through the prism of the Kolmogorov length scale, which is the smallest possible length scale (l_k) before dissipation of eddies in the form of heat,[50]

$$l_k = (\eta^3/\varepsilon)^{1/4}, \tag{3}$$

where η and ε are the kinematic viscosity and the energy dissipation rate per unit mass (or energy mass density), respectively.

Previous studies showed a good correlation between turbulent surface waves on the surface and the Kolmogorov power spectrum.[42,47,51] An increase in energy input increases the energy dissipation rate and consequently results in a shorter wavelength, which is consistent with our observations as indicated by the function $P^{-1/4}$ drawn as a line in Fig. 3(a) (having considered a linear relation between input power and kinetic energy).

These results demonstrate that the surface wavelengths of a SAW activated droplet are strongly related to the characteristic length scale (i.e., the diameter) of the droplet itself [blue squares in Fig. 2(a)]. This provides a new strategy for controlling the formation of surface waves, i.e., by adjusting the liquid's characteristic length scale, which itself can be achieved by confining the liquid in defined geometries. To further develop this capability, we have explored the use of micro-grids as "low-pass" wave filters (Sec. III B) and investigated how this affected the droplet size of aerosols obtained through SAW nebulisation (Sec. III C).

B. Low pass surface wave filter

Our strategy for controlling the formation of surface waves by adjusting the liquid's characteristic length scale was achieved by constraining the liquid in defined geometries by means of microcavities of different diameters fabricated in silicon plates, all with same depth of circa 250 μm. The cavities were filled with water [as depicted in Fig. 1(b)] and excited by SAWs at a frequency of 9.9 MHz. The deformation of the liquid surface was monitored with a high-speed camera [Fig. 1(d)].

Figure 4 shows single frames extracted from videos capturing the confined waves within filters of 1500, 800, and 200 μm in diameter (videos are available in the supplementary material). We observed that the mean surface wavelength decreased with filter diameter [Fig. 2(a), diamonds]. In particular, it is interesting to highlight that the surface waves within the largest confinement (1500 μm) were found to be of similar size to those occurring on a free (unconfined or sessile) liquid surface [Figs. 2(b) and 2(c)] and show a peak of 200 μm with a shoulder at 350 μm [highlighted with an arrow

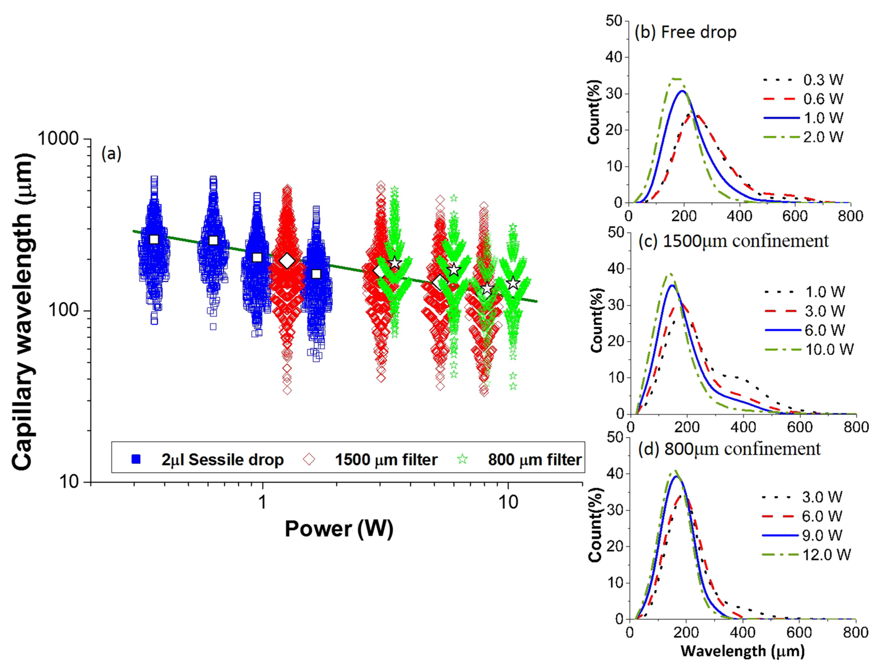

FIG. 3. (a) Variation in mean wavelength against input power for the cases of a sessile drop (blue square), a micro-grid filter 1500 μm in diameter (red diamond), and a filter 800 μm in diameter (green star); the line indicates variation in Kolmogorov length scale with input energy (i.e., $l_k \propto P^{-1/4}$). The width of the scatter plots is to ease reading and does not represent measurement—each population is only linked to one characteristic length scale. [(b)–(d)] Measured wavelength distributions for sessile droplet and liquid confined in cavities. (b) Variation in surface wave spectrum (bin size 50 μm) with input power for a 2.0 μl droplet (1.6 mm) of water; dotted black line: 0.3 W; dashed red line: 0.6 W; solid blue line: 1.0 W; and dotted-dashed green line: 2.0 W. (c) Surface wave spectrum for various energy inputs for liquid confined within 1500 μm cavity: black dotted line: 1 W; red dashed line: 3 W; blue solid line: 6 W; and green dotted-dashed line: 10 W. (d) Variation in wavelength with input power for confined liquids in 800 μm cavity excited with various input powers (black dotted line: 3 W; red dashed line: 6 W; blue solid line: 9 W; and green dotted-dashed line: 12 W).

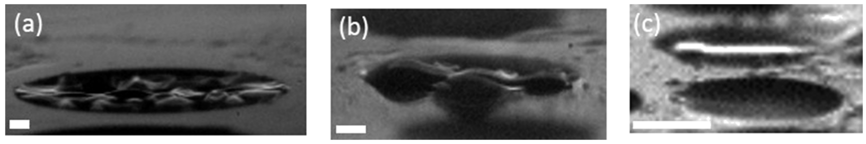

FIG. 4. Surface waves on the surface of liquid confined within cavities of diameter of (a) 1500 μm, (b) 800 μm, and (c) 200 μm. Scale bar on all figures is 100 μm. Images extracted from videos 1–3 are available in the supplementary material.

in Fig. 2(c)]. By decreasing the confinement size to 800 μm, the number of long waves (ca. 500 μm) decreased. A further decrease in the cavity of filter size to 600 and 400 μm results in a further decrease in long surface waves and also shift of peak toward 150 μm [Fig. 2(c)]. The longest measured surface wavelength in these filters was ca. 300 μm. Figure 4 highlights the effect of physical confinement on the surface waves.

In order to explain the above mentioned relationship, we consider a physically confined body of length L (Fig. 5). A two-dimensional surface wave on the liquid [introduced in Eq. (1)] has a velocity potential of $\phi = A\cos(kx - \omega t)\cosh(y + h)$.[32,33] The waves (in the x-direction) reflect at the boundary and the horizontal velocity then takes the form of two waves moving in different directions (positive and negative ω) and two amplitudes as ($U = \frac{\partial\phi}{\partial x}$)

$$U(x) = A_1 k\cosh(h)\sin(kx - \omega t) - A_2 k\cosh(h)\sin(kx + \omega t).$$

Assuming no energy loss in the reflection at the boundary implies $A_1 = A_2 = A$, and the velocity can be rewritten as

$$U(x) = 2Ak\cosh(h)\sin(kx)\cos(\omega t).$$

The second boundary condition linked to the confinement stipulates that there is no movement at the boundary $U(x_0) = U(L) = 0$ that yields $\sin(kL) = 0$. Under these conditions, k should be in form of $k = n\pi/L$ (where n is an integer value) and

$$\lambda = \frac{2\pi}{k} = \frac{2}{n}L. \tag{4}$$

The peak values of the surface wavelength spectrum for all cavities show the harmonics described by Eq. (4). These values correspond to n = 15, 8, 8, and 6th harmonics for cavities with a diameter of 1500, 800, 600, and 400 μm, respectively [Figs. 2(b) and 2(c)]. When a cavity size of 200 μm in diameter was used, standing waves at $\lambda = L$ were observed [Fig. 4(c)].

As observed for free surfaces [see Fig. 3(a)] and also discussed above, the acoustic excitation power is a useful parameter to control the distribution of surface waves towards smaller wavelengths. By varying the power input for cavities of 1500 and 800 μm in diameter, we demonstrate that a higher input power does result in a decrease in surface wave wavelength [Fig. 3(a)] as expected. The proportion of long surface waves also decreases and the peak of distributions shifts towards shorter waves. For instance, in the case of a 1500 μm cavity, an increase in the input power from 1.0 to 3.0 W reshaped the bi-modal distribution into a right-skewed one; which for higher powers (i.e., 6 W and 10 W), transforms into a sharp mono-modal distribution with a lower mode [Fig. 3(c)]. The same trend was observed for a filter with cavities of diameter 800 μm. However, in this case, a broader peak can be observed, which indicates the excitation of a wide range of harmonics (n = 8–12) for higher values of energy input [Fig. 3(d)].

The excitation of higher harmonics at high acoustic input powers can be correlated to an extrapolation of the Kolmogorov length scale, enabling access to shorter waves in the energy cascade of a turbulent wave. The Kolmogorov length scale [Eq. (3)] can be rewritten by considering the mechanisms for energy dissipation, which can be related to the largest length scale of the system as follows:[52]

$$\varepsilon \sim \frac{v^2}{L/v} \sim \frac{v^3}{L} \tag{5}$$

yielding a Kolmogorov length scale of

$$l_k \sim (\frac{\eta^3 L}{v^3})^{1/4}, \tag{6}$$

where l_k is now directly related to the liquid characteristic length scale of the filter ($\sim L^{1/4}$) and inversely related to the velocity $\sim v^{-3/4}$, which is proportional to the input power (P).

This model explains the observed trends in the cases of both small cavities (i.e., small L, Fig. 2) and high powers (i.e., high v) that produce short surface waves [Fig. 3(a)]. These observations confirm that higher harmonics and surface waves with shorter wavelengths can be achieved through either applying a higher input power or decreasing the liquid characteristic length scale [Figs. 2(a) and 5]. However, a sharper distribution of surface wave wavelengths was achieved through physical confinement compared to higher input power, as can be seen from a comparison between the mean and median values of the surface wavelengths' distributions. It is important to highlight that although the increase in input power produces short

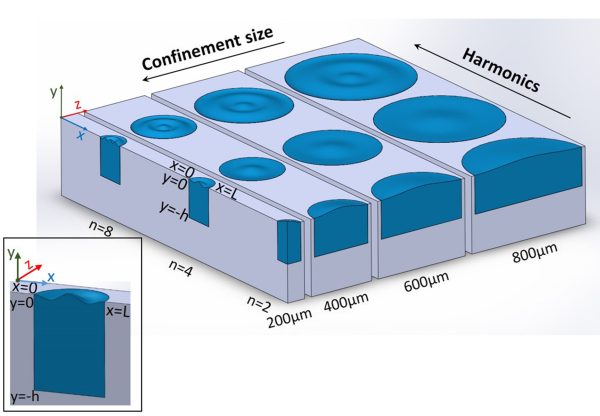

FIG. 5. A schematic representation of capillary waves within filters (physical confinements) having different cavity sizes (each row is a representative of a specific filter with a cavity size—in practice, one surface only has one size), showing changes in capillary wavelength with filter size and harmonics. Inset shows a close-up of the wave on the surface.

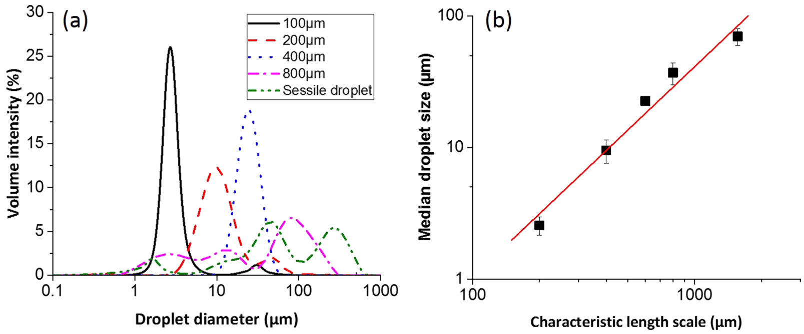

FIG. 6. (a) Droplet size distribution with cavity size for droplets formed from green dashed dot 2 μl droplet (i.e., 1.6 mm), pink dashed dot: 800 μm; blue dotted: 400 μm; red dashed: 200 μm; and black solid line: 100 μm. Applied acoustic power for the case of a sessile droplet is 2 W and 12 W for all confined structures. (b) Median droplet size Dv(50) with the liquid's characteristic length scale (i.e., droplet diameter or cavity diameter). Error bars shows standard deviation from at least three measurements. The line is the linear best fit of the data, slope 1.6.

surface waves, it does not necessarily result in the disappearance of long surface waves. Therefore, to obtain smaller drops, it is more advantageous to confine the liquid and use input power to further refine the specific size required for a specific application.

C. Droplet size of aerosols obtained through SAW nebulisation

As stated, previous reports have correlated the final droplet size from SAW nebulisation to the capillary wave resonant frequency and wavelength.[6,35,39,42] The physical confinement of the liquid using different sizes of cavities provides us with the ability to restrict the sizes of nebulised droplets in the aerosol by controlling the surface wave wavelength. The aerosol droplet size of nebulised liquid from various confinement sizes was measured using laser diffraction, and their median droplet size and droplet size distribution are reported in Fig. 6. The median aerosol droplet size decreases as the confinement diameter decreases [Fig. 6(b)]. This was consistent with our earlier observation of the formation of surface waves with short wavelength within small cavities. The droplet size distribution of aerosols yielded from confined liquid shows a large decrease in distribution width and formation of aerosols with relatively sharper distributions compared to a free water droplet [Fig. 6(a)]. A decrease in the formation of large droplets was visible for cavities with a size of 800 μm in diameter. Decreasing the cavity diameter to 400 μm led to the formation of an aerosol with a mono-modal distribution and a peak in the range of 20 μm. Further decrease in physical confinement diameter to 200 μm and 100 μm showed a further decrease in the peak to below 10 and 2 μm. The latter value lies within the desirable range of aerosol droplet size for pulmonary drug delivery. The best linear fit of the data shown in Fig. 6(b) has a slope of 1.6. Although the decrease in median droplet size with liquid length shows a similar trend to that of the wavelength of the surface waves, it has a different power law. The complex process of drop formation during nebulisation is a result of chaotic flows and surface detachment,[7,53] and it is known to depend on a large number of parameters including viscosity, surface tension, and acoustic wave propagation. The precise relationship has not been established yet and will form the basis of future studies.

The size of the drops present in the aerosol has also been linked to the thickness of the liquid on free surfaces.[7,54] In a confined situation, shallow structures lead to the liquid spreading out of the confinement, whereas deep confinements can increase the sound wave attenuation, yielding less vibration on the surface of liquid.

IV. CONCLUSION

Previous reports have shown a correlation between wavelength on the surface of liquid and median droplet size of the resulting aerosol. In this report, we now show that by controlling the liquid length scale, we can manipulate the waves on the surface of a vibrating liquid and consequently the size of the nebulised droplets. This is evidenced by nebulisation of different volumes excited by means of surface acoustic waves on the surface of an interdigitated transducer, for which shorter surface waves were formed on smaller droplets. We also demonstrated the use of a series of surface wave filters (micro-fabricated on disposable chips) with different cavity sizes to confine the vibrating liquid and enhance the control of the wavelength.

By using the Kolmogorov length scale, it is also shown that shorter wavelength and higher harmonics can be accessed through both smaller physical confinements and increased power. Finally, the median droplet size and droplet size distribution of resulting aerosols from these confinements were measured and showed a decrease with confinement size, indicating a correlation between capillary wavelengths and resulting droplets. Control over final droplet size and droplet size distribution was achieved using the physical confinement and droplets with median diameter in the desired range of 2 μm for optimal delivery of drugs in pulmonary diseases.[20,21]

SUPPLEMENTARY MATERIAL

Videos of Fig. 4 are provided as supplementary material.

ACKNOWLEDGMENTS

This work was supported by an EPSRC Grant (No. EP/K027611/1) and an ERC Advanced Investigator Award (340117 Biophononics). J.R. acknowledges the University of Glasgow Lord Kelvin and Adam Smith Research Fellowship.

APPENDIX: DATA AVAILABILITY

All data are available with open access at https://doi.org/10.5525/gla.researchdata.496.

[1]J. Reboud, Y. Bourquin, R. Wilson, G. S. Pall, M. Jiwaji, A. R. Pitt, A. Graham, A. P. Waters, and J. M. Cooper, "Shaping acoustic fields as a toolset for microfluidic manipulations in diagnostic technologies," Proc. Natl. Acad. Sci. U. S. A. **109**, 15162 (2012).
[2]J. Reboud, R. Wilson, Y. Zhang, M. H. Ismail, Y. Bourquin, and J. M. Cooper, "Nebulisation on a disposable array structured with phononic lattices," Lab Chip **12**, 1268 (2012).
[3]Y. Bourquin, R. Wilson, Y. Zhang, J. Reboud, and J. M. Cooper, "Phononic crystals for shaping fluids," Adv. Mater. **23**, 1458 (2011).
[4]M. A. Khalid, J. Reboud, R. Wilson, and J. M. Cooper, "Control of blood's rheological properties using surface acoustic waves," in *17th International Conference on Miniaturized Systems for Chemistry and Life Sciences* (RSC Publishing Ltd., 2013), pp. 101–103, ISBN: 978-0-9798064-6-9.
[5]K. Tveen-Jensen, F. Gesellchen, R. Wilson, C. M. Spickett, J. M. Cooper, and A. R. Pitt, "Interfacing low-energy SAW nebulization with liquid chromatography-mass spectrometry for the analysis of biological samples," Sci. Rep. **5**, 9736 (2015).
[6]Y.-J. Chen and P. H. Steen, "Dynamics of inviscid capillary breakup: Collapse and pinchoff of a film bridge," J. Fluid Mech. **341**, 245 (1997).
[7]D. J. Collins, O. Manor, A. Winkler, H. Schmidt, J. R. Friend, and L. Y. Yeo, "Atomization off thin water films generated by high-frequency substrate wave vibrations," Phys. Rev. E: Stat., Nonlinear, Soft Matter Phys. **86**, 056312 (2012).
[8]Q. Zhou, L. Qu, T. Gengenbach, I. Larson, P. J. Stewart, and D. A. V. Morton, "Effect of surface coating with magnesium stearate via mechanical dry powder coating approach on the aerosol performance of micronized drug powders from dry powder inhalers," AAPS PharmSciTech **14**, 38 (2013).
[9]J.-W. Kim, Y. Yamagata, M. Takasaki, B.-H. Lee, H. Ohmori, and T. Higuchi, "A device for fabricating protein chips by using a surface acoustic wave atomizer and electrostatic deposition," Sens. Actuators, B **107**, 535 (2005).
[10]E. Babinsky and P. E. Sojka, "Modeling droplet size distribution," Prog. Energy Combust. Sci. **28**, 303 (2002).
[11]A. Qi, P. Chan, J. Ho, A. Rajapaksa, J. Friend, and L. Yeo, "Template-free synthesis and encapsulation technique for layer-by-layer polymer nanocarrier fabrication," ACS Nano **5**, 9583 (2011).
[12]S. R. Heron, R. Wilson, S. A. Shaffer, D. R. Goodlett, and J. M. Cooper, "Surface acoustic wave nebulization of peptides as a microfluidic interface for mass spectrometry," Anal. Chem. **82**, 3985 (2010).
[13]J. Ho, M. K. Tan, D. B. Go, L. Y. Yeo, J. R. Friend, and H.-C. Chang, "Paper-based microfluidic surface acoustic wave sample delivery and ionization source for rapid and sensitive ambient mass spectrometry," Anal. Chem. **83**, 3260 (2011).
[14]A. Mar, J. Friend, and L. Y. Yeo, "Rapid generation of protein aerosols and nanoparticles via surface acoustic wave atomization," Nanotechnology **19**, 455103 (2008).
[15]N. K. Verma, K. Crosbie-Staunton, A. Satti, S. Gallagher, K. B. Ryan, T. Doody, C. McAtamney, R. MacLoughlin, P. Galvin, C. S. Burke, Y. Volkov, and Y. K. Gun'ko, "Magnetic core-shell nanoparticles for drug delivery by nebulization," J. Nanobiotechnol. **11**, 1 (2013).
[16]A. E. Rajapaksa, J. J. Ho, A. Qi, R. Bischof, T.-H. Nguyen, M. Tate, D. Piedrafita, M. P. McIntosh, L. Y. Yeo, E. Meeusen, R. L. Coppel, and J. R. Friend, "Effective pulmonary delivery of an aerosolized plasmid DNA vaccine via surface acoustic wave nebulization," Respir. Res. **15**, 1 (2014).
[17]A. Qi, J. R. Friend, L. Y. Yeo, D. A. V. Morton, M. P. McIntosh, and L. Spiccia, "Miniature inhalation therapy platform using surface acoustic wave microfluidic atomization," Lab Chip **9**, 2184 (2009).
[18]E. R. Society, European Lung White Book, http://www.erswhitebook.org/chapters/the-burden-of-lung-disease/.
[19]G. J. Gibson, R. Loddenkemper, B. Lundbäck, and Y. Sibille, "Respiratory health and disease in Europe: The new european lung white book," Eur. Respir. J. **42**, 559 (2013).
[20]M. Ibrahim, R. Verma, and L. Garcia-Contreras, "Inhalation drug delivery devices: Technology update," Med. Devices: Evidence Res. **8**, 131 (2015).
[21]J. Heyder, "Deposition of inhaled particles in the human respiratory tract and consequences for regional targeting in respiratory drug delivery," Proc. Am. Thorac. Soc. **1**, 315 (2004).
[22]A. Beer, "Bestimmung der Absorption des rothen Lichts in farbigen Flüssigkeiten," Ann. Phys. **162**, 78–88 (1852).
[23]J. Plateau, *Experimental and Theoretical Statics of Liquids Subject to Molecular Forces Only* (Gauthier-Villars, Paris, 1873).
[24]Lord Rayleigh, "On the instability of jets," Proc. London Math. Soc. **s1-10**, 4–13 (1878).
[25]Lord Rayleigh, "On the capillary phenomena of jets," Proc. R. Soc. London **29**, 71 (1879).
[26]J. Eggers, J. R. Lister, and H. A. Stone, "Coalescence of liquid drops," J. Fluid Mech. **401**, 293 (1999).
[27]L. Duchemin, S. Popinet, C. Josserand, and S. Zaleski, "Jet formation in bubbles bursting at a free surface," Phys. Fluids **14**, 3000 (2002).
[28]F. H. Zhang, M. J. Thoraval, S. T. Thoroddsen, and P. Taborek, "Partial coalescence from bubbles to drops," J. Fluid Mech. **782**, 209 (2015).
[29]J. M. López-Herrera, P. Riesco-Chueca, and A. M. Gañán-Calvo, "Linear stability analysis of axisymmetric perturbations in imperfectly conducting liquid jets," Phys. Fluids **17**, 034106 (2005).
[30]I. M. Wallwork, S. P. Decent, A. C. King, and R. M. S. M. Schulkes, "The trajectory and stability of a spiralling liquid jet. Part 1. Inviscid theory," J. Fluid Mech. **459**, 43 (2002).
[31]S. C. Tsai, S. K. Lin, R. W. Mao, and C. S. Tsai, "Ejection of uniform micrometer-sized droplets from Faraday waves on a millimeter-sized water drop," Phys. Rev. Lett. **108**, 154501 (2012).
[32]L. D. Landau and E. M. Lifshitz, *Fluid Mechanics* (Pergamon Press, Edinburgh, London, 1987).
[33]D. J. Acheson, *Elementary Fluid Dynamics* (Oxford University Press, Norfolk, Great Britain, 1990).
[34]C. L. Goodridge, W. T. Shi, and D. P. Lathrop, "Threshold dynamics of singular gravity-capillary waves," Phys. Rev. Lett. **76**, 1824 (1996).
[35]R. J. Lang, "Ultrasonic atomization of liquids," J. Acoust. Soc. Am. **34**, 6 (1962).
[36]J. N. Antonevich, "Ultrasonic atomization of liquids," IRE Trans. Ultrason. Eng. **PGUE-7**, 6 (1959).
[37]W. Eisenmenger, "Dynamic properties of the surface tension of water and aqueous solutions of surface active agents with standing capillary waves in the frequency range from 10 kc/s to 1.5 Mc/s," Acustica **9**, 327 (1959).
[38]J. W. S. Rayleigh, *The Theory of Sound* (Dover Publications, New York, 1954).
[39]J. Ju, Y. Yamagata, H. Ohmori, and T. Higuchi, "Standing wave type surface acoustic wave atomizer," Sens. Actuators, A **147**, 570 (2008).
[40]J. Ju, Y. Yamagata, H. Ohmori, and T. Higuchi, "High-frequency surface acoustic wave atomizer," Sens. Actuators, A **145-146**, 437 (2008).
[41]M. Kurosawa, T. Watanabe, A. Futami, and T. Higuchi, "Surface acoustic wave atomizer," Sens. Actuators, A **50**, 69 (1995).
[42]A. Qi, L. Y. Yeo, and J. R. Friend, "Interfacial destabilization and atomization driven by surface acoustic waves," Phys. Fluids **20**, 074103 (2008).
[43]J. H. Moon, B. H. Kang, and H.-Y. Kim, "The lowest oscillation mode of a pendant drop," Phys. Fluids **18**, 021702 (2006).
[44]O. Manor, A. R. Rezk, J. R. Friend, and L. Y. Yeo, "Dynamics of liquid films exposed to high-frequency surface vibration," Phys. Rev. E **91**, 053015 (2015).
[45]J. Blamey, J. R. Friend, and L. Y. Yeo, *Acoustically Induced Micro-Scale Capillary Wave Turbulence* (ICA, Sydney, Australia, 2010).
[46]E. Trinh and T. G. Wang, "Large-amplitude free and driven drop-shape oscillations: Experimental observations," J. Fluid Mech. **122**, 315 (1982).
[47]J. Blamey, L. Y. Yeo, and J. R. Friend, "Microscale capillary wave turbulence excited by high frequency vibration," Langmuir **29**, 3835 (2013).
[48]C. Witte, J. Reboud, R. Wilson, J. M. Cooper, and S. L. Neale, "Microfluidic resonant cavities enable acoustophoresis on a disposable superstrate," Lab Chip **14**, 4277 (2014).
[49]M. K. Tan, J. R. Friend, O. K. Matar, and L. Y. Yeo, "Capillary wave motion excited by high frequency surface acoustic waves," Phys. Fluids **22**, 112112 (2010).
[50]E. Nazarzadeh and S. Sajjadi, "Viscosity effects in miniemulsification via ultrasound," AIChE J. **56**, 2751 (2010).
[51]A. N. Pushkarev and V. E. Zakharov, "Turbulence of capillary waves—Theory and numerical simulation," Phys. D **135**, 98 (2000).
[52]S. B. Pope, *Turbulent Flows* (Cambridge University Press, New York, 2000).
[53]E. Jens and V. Emmanuel, "Physics of liquid jets," Rep. Prog. Phys. **71**, 036601 (2008).
[54]M. K. Tan, J. R. Friend, and L. Y. Yeo, "Interfacial jetting phenomena induced by focused surface vibrations," Phys. Rev. Lett. **103**, 024501 (2009).